JACS
JOURNAL OF THE AMERICAN CHEMICAL SOCIETY

ARTICLE

pubs.acs.org/JACS

Divided-Evolution-Based Pulse Scheme for Quantifying Exchange Processes in Proteins: Powerful Complement to Relaxation Dispersion Experiments

Guillaume Bouvignies, D. Flemming Hansen,*,† Pramodh Vallurupalli, and Lewis E. Kay*

Departments of Molecular Genetics, Biochemistry, and Chemistry, The University of Toronto, Toronto, Ontario, Canada M5S 1A8

Supporting Information

ABSTRACT: A method for quantifying millisecond time scale exchange in proteins is presented based on scaling the rate of chemical exchange using a 2D ^{15}N, ^{1}H^{N} experiment in which ^{15}N dwell times are separated by short spin-echo pulse trains. Unlike the popular Carr−Purcell−Meiboom−Gill (CPMG) experiment where the effects of a radio frequency field on measured transverse relaxation rates are quantified, the new approach measures peak positions in spectra that shift as the effective exchange time regime is varied. The utility of the method is established through an analysis of data recorded on an exchanging protein−ligand system for which the exchange parameters have been accurately determined using alternative approaches. Computations establish that a combined analysis of CPMG and peak shift profiles extends the time scale that can be studied to include exchanging systems with highly skewed populations and exchange rates as slow as 20 s^{-1}.

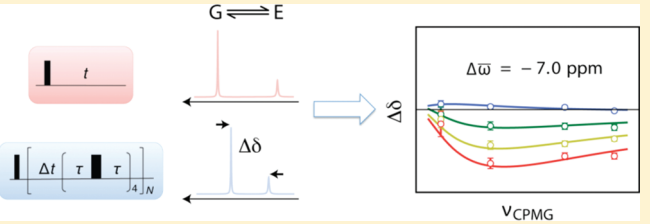

INTRODUCTION

Carr−Purcell−Meiboom−Gill (CPMG) relaxation dispersion NMR spectroscopy[1,2] has become a very powerful method for detailed studies of proteins that exchange between a highly populated, "visible" ground state and one or more lowly populated and generally "invisible" excited states.[3−6] As long as the exchange rate is on the millisecond time scale and excited states are populated at levels of 0.5% or higher, the effective relaxation rates of the ground-state nuclei, $R_{2,\mathrm{eff}}$, can be modulated by the application of a spin-echo pulse train where the intervals between successive refocusing pulses, 2τ, are varied.[3] Subsequent fits of the resulting dispersion profiles, $R_{2,\mathrm{eff}}$ vs $\nu_{\mathrm{CPMG}} = 1/(4\tau)$, lead to the extraction of populations of the exchanging states and rates of exchange along with absolute values of the chemical shift differences between the interconverting conformers.[3] Backbone chemical shifts of lowly populated states are particularly valuable because they provide an avenue for structure determination when used in concert with robust computational database approaches such as CS-Rosetta,[7] CHESHIRE,[8] and CS23D.[9] With this in mind, optimized labeling methods and dispersion experiments tailored to the type of label have been developed for measuring ^{15}N (refs 10−12), ^{1}H^{N} (ref 13) ^{13}C$^{\alpha}$ (ref 14), ^{13}CO (refs 15 and 16), ^{13}C$^{\beta}$ (ref 17), and ^{1}H$^{\alpha}$ (ref 18) chemical shifts of excited states. Recently, an atomic resolution structural model of a lowly populated folding intermediate of an FF domain was published based on chemical shifts and residual dipolar coupling values that were measured by CPMG-based methods.[19]

CPMG and the related $R_{1\rho}$ class of experiments exploit the fact that the effective chemical shift difference between exchanging spins can be modulated by applying a $\mathbf{B}_1$ field of varying strength, leading to quantifiable changes in transverse relaxation rates of ground-state spins. It is also possible to imagine other types of experiments, however, that focus instead on modulating the resonance position of ground-state nuclei, which, like relaxation rates, also depends on exchange parameters.[20,21] Fits of peak positions, rather than transverse relaxation rates, then provide measures of exchange rates, populations, and signed chemical shift differences. Here we describe a divided evolution-based pulse scheme that follows from earlier studies of Morris and coworkers[22] and subsequently Zhuravleva and Orekhov,[23] in which each dwell point in the indirect detection period of a two-dimensional HSQC experiment is separated by an element comprised of a constant number of spin echoes. Modulation of peak positions is achieved by changing either the t_1 dwell time, Δt (i.e, the F_1 spectral width) or the time between successive refocusing pulses in each spin-echo element or both in a manner outlined below. The methodology is validated through studies of a protein−ligand exchanging system that has been characterized previously using CPMG experiments and that can be manipulated by the addition of different amounts of ligand to generate spectra of the "ground" (ligand-free) or "excited" (ligand-bound) states.[24] Excellent agreement is noted between the signed chemical shift differences obtained from fits of peak positions and the corresponding shift differences generated independently. It is shown that in some cases the divided evolution (D-evolution) experiment has important advantages over the conventional CPMG

Received: October 25, 2010
Published: January 18, 2011

scheme. Moreover, simulations establish that a combined analysis of CPMG and D-evolution profiles can expand the exchange time scale window that is amenable to study to include exchange processes with rates as low as 20 s^{-1} and populations of excited states that are several percent.

RESULTS AND DISCUSSION

Theoretical Considerations. To understand the underlying principles behind the D-evolution experiment[22,23] for quantifying chemical exchange, we consider a system exchanging between two states

$$A \underset{k_{BA}}{\overset{k_{AB}}{\rightleftarrows}} B$$

with $p_B \ll p_A$, where p_j is the fractional population of state j. The evolution of magnetization during an interval of free precession can be expressed as

$$\frac{d}{dt}\begin{bmatrix} M_+^A \\ M_+^B \end{bmatrix} = \begin{bmatrix} -k_{AB} - R_2 & k_{BA} \\ k_{AB} & -k_{BA} + i\Delta\omega - R_2 \end{bmatrix}\begin{bmatrix} M_+^A \\ M_+^B \end{bmatrix} \quad (1)$$

where $M_+ = M_X + iM_Y$, with M_j the j component of magnetization, $\Delta\omega$ is the difference in chemical shifts between exchanging nuclei (rad/s), and the intrinsic transverse relaxation rates of spins in both states are assumed equal, R_2. Without loss in generality, the chemical shift of site A (i.e., the peak position in the absence of chemical exchange) is set to 0. The time evolution of magnetization can be readily calculated by integration of eq 1:

$$\begin{bmatrix} M_+^A(t) \\ M_+^B(t) \end{bmatrix} = \exp(\mathbf{\Lambda} t)\begin{bmatrix} M_+^A(0) \\ M_+^B(0) \end{bmatrix} \quad (2)$$

where $\mathbf{\Lambda}$ is the matrix on the right-hand side of eq 1. Chemical exchange introduces a shift in the resonance positions of the exchanging spins so that in a simple pulse-acquire ($90°-t$) experiment the peak position for state A is offset from its position in the absence of exchange (ω_A, assumed zero in eq 1 above) in the amount[20,21]

$$\Delta\delta_{ex} \approx k_{AB}\frac{\zeta}{1+\zeta^2} \qquad \zeta = \frac{\Delta\omega}{k_{BA}} \quad (3)$$

Equation 3 makes it clear that, as the exchange time scale increases, from the slow exchange limit, $k_{ex} = k_{AB} + k_{BA} \ll \Delta\omega$, where $\Delta\delta_{ex} \approx p_A p_B \Delta\omega (k_{ex}/\Delta\omega)^2$, to the fast exchange limit, $k_{ex} \gg \Delta\omega$ and $\Delta\delta_{ex} \approx (p_B/p_A)\Delta\omega$, the peak position "migrates" with a maximum in $\Delta\delta_{ex}$ under conditions of fast exchange.

Consider now the D-evolution scheme,[22,23] which differs from the pulse-acquire experiment in that the detection of magnetization occurs during a series of N equal periods, each corresponding to a single dwell point ($\Delta t = t/N$), with each dwell separated by an element of duration T_{CPMG}, $90°(-\Delta t - T_{CPMG}-)_N$, with $T_{CPMG} = (-\tau - 180° - \tau -)_4$, Figure 1a. The choice of four echoes per element is based on practical considerations: it ensures that a minimum four-step phase cycle can be employed for the 180° pulses that is necessary to avoid artifacts (see below). A D-evolution scheme has been reported previously for chemical shift scaling[22] and subsequently to narrow lines that are significantly broadened due to chemical exchange.[23] We show here that it can also be used in a very different manner to modulate the position of peaks, which in turn provides an avenue for measuring chemical exchange parameters. The modulation is shown in Figure 1b where the shift of the resonance line of spin A relative to its position in the pulse-acquire experiment is calculated numerically for a two-site exchanging system described in the figure caption. We will show subsequently that such profiles can be fit to extract exchange parameters and *signed* chemical shift differences, in a manner analogous to fits of CPMG dispersion profiles, although in that case only absolute values of shift differences are measured. Our immediate goal, however, is to present a qualitative description so that the main features of Figure 1b can be understood "intuitively".

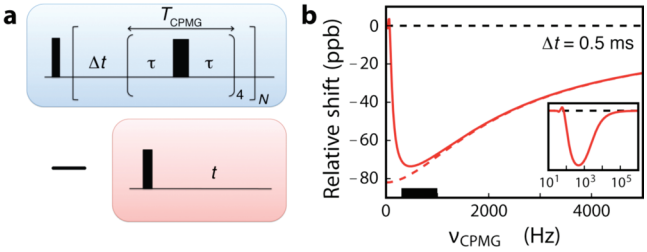

Figure 1. (a) 1D version of the basic D-evolution scheme described in the text (blue) along with a "standard" pulse-acquire experiment (red). The detection of magnetization in the D-evolution scheme occurs during a series of N equal periods, each corresponding to a single dwell point ($\Delta t = t/N$), that are separated from each other by an element of duration $T_{CPMG} = (-\tau - 180° - \tau -)_4$. The experimental parameter of interest is the difference in positions of corresponding peaks in spectra obtained with the D-evolution and standard experiments. (b) Simulated profile of the relative ^{15}N shift of the major state ("A") correlation in a two-site exchanging system, A $\rightleftarrows$ B, calculated as the difference in the corresponding peak positions in D-evolution and pulse-acquire experiments as a function of $\nu_{CPMG} = 1/(4\tau)$, with $\Delta t = 0.5$ ms. Parameters used in the simulation are $p_B = 5\%$, $k_{ex} = 300\ s^{-1}$, $\Delta\tilde{\omega} = -2$ ppm (^{15}N), and 11.7 T. The black box on the x-axis highlights the range of ν_{CPMG} values that are typically accessible experimentally, with the inset showing a larger ν_{CPMG} range to emphasize the dependence of the relative shift on ν_{CPMG}. The dashed red line is calculated from eq 5, as described in the text.

The net effect of the scheme of Figure 1a (highlighted in blue) on magnetization evolution can be calculated according to

$$\begin{bmatrix} M_+^A(T_{CPMG} + \Delta t) \\ M_+^B(T_{CPMG} + \Delta t) \end{bmatrix} = \{\exp(\mathbf{\Lambda}\tau)\exp(\mathbf{\Lambda}^* 2\tau)\exp(\mathbf{\Lambda}\tau)\}^2 \exp(\mathbf{\Lambda}\Delta t)\begin{bmatrix} M_+^A(0) \\ M_+^B(0) \end{bmatrix} \quad (4)$$

where $8\tau = T_{CPMG}$ and $\mathbf{\Lambda}^*$ is a matrix obtained from $\mathbf{\Lambda}$ by replacing $i\Delta\omega$ by $-i\Delta\omega$. Analytical expressions for both the major (visible) state peak position and the time dependence of magnetization in terms of rates and chemical shift differences that are valid for all τ and Δt are complicated. However, it is straightforward to consider a pair of limiting cases, $\nu_{CPMG} \rightarrow 0$ and $\nu_{CPMG} \rightarrow \infty$, even if such cases are not achieved in practice. In the case where ν_{CPMG} is close to 0, $\tau = (1/8)T_{CPMG}$ is large, and for $\tau \gg 1/k_{AB}$, $1/k_{BA}$, and $1/\Delta\omega$, magnetization evolves during each of the τ periods according to eq 1. Since the application of each 180° pulse during T_{CPMG} is equivalent to inversion of the sign of $\Delta\omega$ for the subsequent duration between pulses, the evolution frequency of M_+^A alternates between $\pm(\omega_A + \Delta\delta_{ex})$ (eq 3) during this period, hence averaging to zero. Thus, between successive dwell points there is no magnetization evolution from exchange or chemical shift: it is as if T_{CPMG} were set to zero, although transverse relaxation does persist. As a consequence, the D-evolution experiment produces no difference in the position of peaks relative to the pulse-acquire scheme, and the relative shift is 0, as

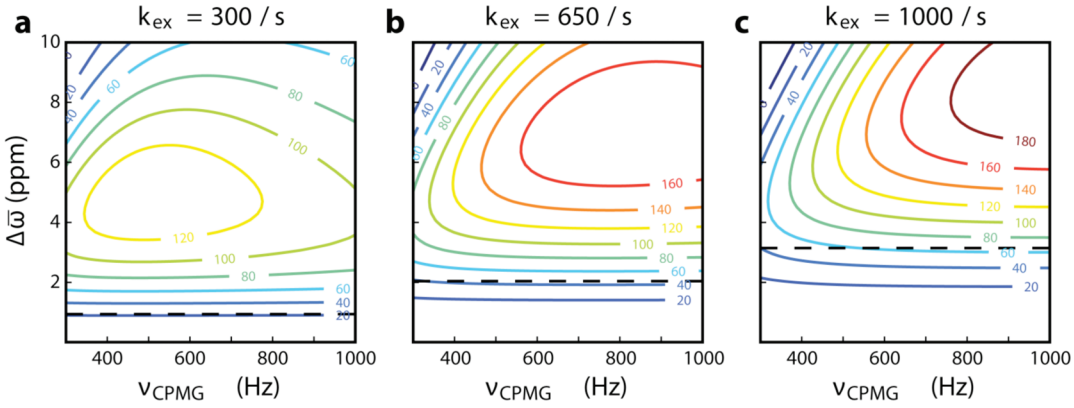

Figure 2. Contour plots showing the relative shift (ppb) between corresponding ^{15}N peak positions in the D-evolution and the simple pulse-acquire experiments, 11.7 T, as a function of $\Delta\tilde{\omega}$ (ppm) and ν_{CPMG} (Hz) for k_{ex} values of 300 (a), 650 (b), and 1000 (c) s^{-1}. The dashed line in each plot corresponds to $\Delta\omega$ (rad/s) = k_{ex}.

in Figure 1b for $\nu_{CPMG} \approx 0$. Of interest, a small oscillatory behavior in shift is observed for low ν_{CPMG} values in cases where $\Delta\omega$ is large, which is reminiscent of what is seen in relaxation dispersion profiles under conditions of slow exchange. In the limit that $\nu_{CPMG} \rightarrow \infty$, τ and hence T_{CPMG} approach 0, so that the CPMG element becomes negligibly small compared to Δt. Thus, the experiment "reverts" to a 90° acquire, and no relative shift is obtained either (inset to Figure 1b).

Between the limiting cases $\nu_{CPMG} \rightarrow 0$ and $\nu_{CPMG} \rightarrow \infty$, the situation is more complex. However, here too the overall features of the shift profile of Figure 1b can be understood by noting that as ν_{CPMG} increases the effective chemical shift difference between exchanging states is scaled down, leading to an increase in the time scale of exchange and hence a relative shift in peak positions (but see below). Consider, for example, the case where refocusing pulses are applied sufficiently rapidly so that $\tau < 1/k_{AB}$, $1/k_{BA}$, and $1/\Delta\omega$ and further that $\Delta t < 1/k_{AB}$, $1/k_{BA}$, and $1/\Delta\omega$. Then, as shown previously by Zhuravleva and Orekhov,[23] only the linear terms in the expansion of each exp(...) term in eq 4 above need be retained, and

$$\begin{bmatrix} M_+^A(T') \\ M_+^B(T') \end{bmatrix} = \begin{bmatrix} 1-(k_{AB}+R_2)T' & k_{BA}T' \\ k_{AB}T' & 1-(k_{BA}+R_2)T'+i\Delta\omega\Delta t \end{bmatrix} \begin{bmatrix} M_+^A(0) \\ M_+^B(0) \end{bmatrix} \quad (5)$$

where $T' = T_{CPMG} + \Delta t = r_D\Delta t$, with $r_D = 1 + T_{CPMG}/\Delta t$. Thus, chemical exchange and chemical shift become "uncoupled" in the sense that the former evolves for the complete time, T', while the latter for only Δt, so that the chemical shift is effectively scaled to zero during the T_{CPMG} period. Hence, relative to chemical shift, chemical exchange has been sped up by the factor r_D, thus increasing the time scale of the exchange process. Since the factors T_{CPMG} and Δt can be varied somewhat (typically, 2 ms $\leq T_{CPMG} \leq$ 7 ms and 0.5 ms $\leq \Delta t \leq$ 2 ms in our applications), the scaling factor r_D is under experimental control; the goal is to record a series of spectra with r_D varied to change the time scale of chemical exchange. Noting that the maximum possible shift of peak A (in a simple pulse-acquire spectrum) occurs in the fast exchange limit, $k_{AB}\zeta$ (see eq 3), the shift in peak position in the D-evolution experiment relative to that in a standard 90° acquire experiment must be smaller than $k_{AB}\zeta[1 - 1/(1 + \zeta^2)]$. The maximum relative shift change (of corresponding peaks in D-evolution and 90° acquire spectra, Figure 1) occurs for a nucleus in slow exchange in free precession ($r_D = 1$), with exchange effectively scaled into the fast regime as r_D increases. In practice the size of the relative shift will depend on the balance between the length of the CPMG element (8τ) and the pulse rate (scaling of $\Delta\omega$); nonzero shifts are obtained when the rate of application of refocusing pulses is sufficiently fast to scale $\Delta\omega$ without being so fast to appreciably reduce the duration of the element. Note that as $\nu_{CPMG} \rightarrow \infty$ the value of T_{CPMG} goes to 0, $r_D \rightarrow 1$, and eq 5 predicts no relative shift, as expected. Equation 5 is only exact in the fast-pulsing, small dwell time limit defined above. However, it provides a reasonable approach for the calculation of magnetization evolution as long as ν_{CPMG} is above a certain threshold that in turn depends on the exchange parameters. The dashed red line in Figure 1b plots relative shifts calculated from eq 5, while the solid red line is the exact shifts from eq 4; for $\nu_{CPMG} > 500$ Hz the agreement is good.

Shown in Figure 2 are contour plots of the relative shift as a function of $\Delta\tilde{\omega}$ (ppm) and ν_{CPMG} for k_{ex} values of 300, 650, and 1000 s^{-1} (11.7 T field, Δt = 0.5 ms). The dashed black line in each plot corresponds to $\Delta\omega$ (rad/s) = k_{ex}. Recalling that large relative shifts are obtained for exchanging systems where the exchange time scale is increased significantly by application of the D-evolution scheme—that is, in cases where exchange is slow/intermediate in the free precession limit—it is not surprising that the position of the maxima in all three plots occurs for $\Delta\omega > k_{ex}$. Further, as k_{ex} and $\Delta\tilde{\omega}$ increase, so too must ν_{CPMG} to maximize the relative shift since higher ν_{CPMG} values are necessary to scale the exchange into the fast regime.

The position of peaks in spectra can also be modulated in the D-evolution scheme by varying the dwell time Δt, as illustrated in Figure 3, where relative shift values are plotted vs ν_{CPMG} for $\Delta\tilde{\omega} = -1$ ppm (a), -2 ppm (b), and -4 ppm (c) and for several values of Δt (0.5 ms, red; 1 ms, green; 2 ms, blue). From eq 5 it becomes clear that as Δt decreases and T_{CPMG} (or ν_{CPMG}) is kept constant the effective exchange time scale increases, leading to larger relative shifts. In practice, several values of Δt and ν_{CPMG} are typically recorded.

Experimental Considerations. Figure 4 illustrates the D-evolution-based pulse scheme for quantifying millisecond time scale chemical exchange in proteins. It is shown below, by simulation, that a combined analysis of D-evolution and CPMG experiments provides a sensitive measure of exchange processes

dx.doi.org/10.1021/ja109589y |J. Am. Chem. Soc. 2011, 133, 1935–1945

on longer time scales, with exchange rates as small as 20 s^{-1} as long as p_B is several percent. The pulse sequence is essentially an $^{15}N-^{1}H$ TROSY-based experiment[25] with the "standard" indirect evolution period replaced by the D-evolution element[22,23] that has been described above and with selection of the ^{15}N TROSY component prior to the t_1 evolution period achieved using an S^3E filter.[26] We have found that to generate high-quality spectra, T_{CPMG} periods must be comprised of a minimum of four echoes, $(-\tau-180_\phi-\tau-)_4$, so that the refocusing pulses can be phase cycled using an *XYXY* scheme. The "basic" four-step echo can be further phase cycled according to an *XY*-16 scheme,[27] as described in the Materials and Methods.

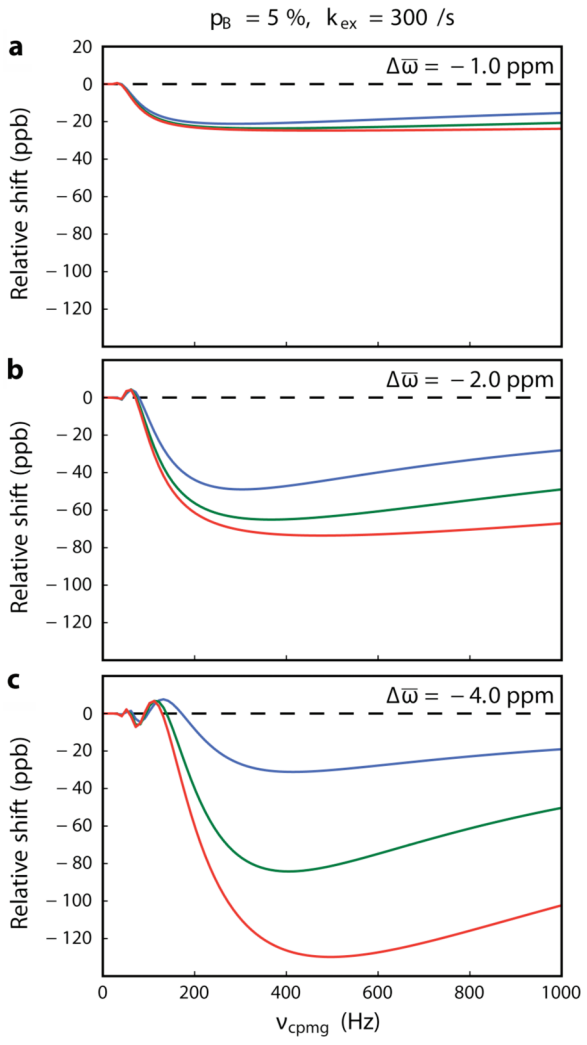

Figure 3. Relative shift profiles (ppb) as a function of ν_{CPMG} (Hz) for $\Delta\tilde{\omega}$ values (^{15}N) of −1.0 (a), −2.0 (b), and −4.0 (c) ppm and Δt values of 2.0 (blue), 1.0 (green), and 0.5 (red) ms. All the calculations were performed assuming an excited-state population of 5%, an exchange rate of 300 s^{-1}, and an external magnetic field of 11.7 T.

The use of a TROSY-based pulse sequence has an important advantage over a non-TROSY experiment that could of course also be constructed to include a D-evolution scheme. Although the exchange time scale is scaled by the D-evolution scheme, eq 5, so too is the relaxation rate, leading to decreased resolution in spectra. It is therefore clearly important that the intrinsic relaxation times of the probe nuclei be as long as possible, facilitating the extraction of accurate chemical shifts. Extracting accurate peak positions also depends on the signal-to-noise ratio of the data sets.[28] This can be improved through the use of highly deuterated protein samples to eliminate amide proton−aliphatic proton scalar couplings while simultaneously increasing intrinsic relaxation times of both amide ^{15}N and ^{1}H spins by minimizing relaxation contributions from protons external to the $^{15}N-^{1}H^{N}$ spin pair in question.

Amide proton relaxation along with solvent exchange (referred to as spin flips below) leads to the interconversion between TROSY and anti-TROSY components,[29] which can introduce significant artifacts, even in the case of highly deuterated samples. In the case of TROSY-based CPMG relaxation dispersion experiments, Palmer and co-workers have introduced an element that effectively refocuses the deleterious effects of TROSY/anti-TROSY exchange, by inverting one of the two components in the center of the CPMG element.[30] Such a scheme is not practical here. Rather, in the experiment of Figure 4 the ^{15}N TROSY magnetization component is selected by an S^3E element[26] that is applied prior to the D-evolution period. We have shown previously in the context of CPMG dispersion experiments that the effects of TROSY/anti-TROSY exchange can be minimized using an approach whereby only the TROSY component is selected at the start of the CPMG element.[31] This works well for the D-evolution experiment as well, as illustrated in Figure 5. Here simulated spectra are presented for a spin system undergoing chemical exchange with k_{ex} = 300 s^{-1} and p_B = 5%, similar to the parameters that are fitted experimentally for the ligand−protein binding system considered below. The interconversion between TROSY and anti-TROSY ^{15}N magnetization components has also been taken into account in the simulation by using an expression similar to eq 1:

$$\frac{d\vec{v}}{dt} = \begin{bmatrix} \mathbf{\Lambda}_{TR} & \mathbf{K} \\ \mathbf{K} & \mathbf{\Lambda}_{ATr} \end{bmatrix} \vec{v}$$

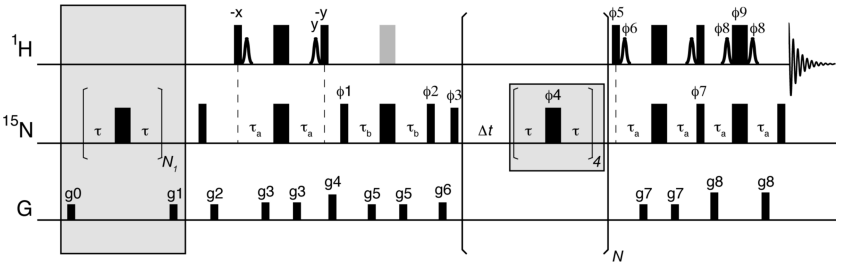

Figure 4. Pulse scheme of the ^{15}N TROSY-based D-evolution experiment for measuring millisecond time scale dynamics in proteins by exchange-induced shift modulation. Details are provided in the Materials and Methods.

dx.doi.org/10.1021/ja109589y |*J. Am. Chem. Soc.* 2011, 133, 1935–1945

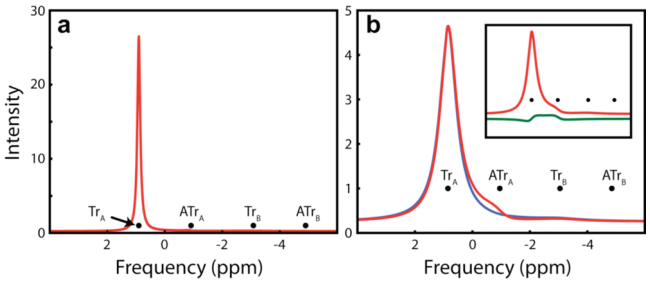

Figure 5. Simulated F_1 (^{15}N) traces from a regular ^{15}N−^{1}H^{N} TROSY data set (a) and a D-evolution TROSY spectrum (b; Δt = 1.0 ms and ν_{CPMG} = 300 Hz) for a spin system undergoing chemical exchange with k_{ex} = 300 s^{-1}, p_B = 5%, R_{sf} = 10 s^{-1}, and a static magnetic field of 11.7 T. The black dots indicate the resonance positions of each of the TROSY (Tr) and anti-TROSY (ATr) lines for both the ground (A) and excited (B) states. The red spectrum in (b) corresponds to the case where the TROSY component is not selected initially, while the blue profile is obtained if the TROSY component is selected prior to evolution (as is done in the experiment of Figure 4 using the S^{3}E element). The inset in (b) shows the case where the anti-TROSY component is selected initially and allowed to evolve under the D-evolution scheme, with selection of TROSY magnetization immediately prior to detection (green), with the red trace of the main figure reproduced for comparison. Note the increased line widths in the D-evolution scheme that manifest from scaling of relaxation rates along with k_{ex}.

where

$$\vec{v} = \begin{bmatrix} M^{A}_{+,Tr} \\ M^{B}_{+,Tr} \\ M^{A}_{+,ATr} \\ M^{B}_{+,ATr} \end{bmatrix} \quad (6)$$

$$\mathbf{\Lambda}_{TR} = \begin{bmatrix} -k_{AB} - R_{2,Tr} - i\pi J & k_{BA} \\ k_{AB} & -k_{BA} + i\Delta\omega - R_{2,Tr} - i\pi J \end{bmatrix} - \mathbf{K}$$

$$\mathbf{K} = \begin{bmatrix} 0.5R_{sf} & 0 \\ 0 & 0.5R_{sf} \end{bmatrix}$$

In eq 6 $R_{2,TR}$ is the intrinsic transverse relaxation rate of the TROSY magnetization component for an isolated ^{15}N−^{1}H^{N} spin system, J is the one-bond ^{15}N−^{1}H^{N} scalar coupling constant, R_{sf} (set to 10 s^{-1} in the simulations of Figure 5) is the TROSY/anti-TROSY exchange rate (spin-flip rate), and $\mathbf{\Lambda}_{ATr}$ is a matrix obtained from $\mathbf{\Lambda}_{Tr}$ by replacing $R_{2,TR}$ by $R_{2,ATr}$, the corresponding transverse relaxation rate for the anti-TROSY component, and $-i\pi J$ by $i\pi J$. Thus, the exchange process considered is essentially a four-site interconversion, although not all sites interchange directly. Figure 5a shows the calculated ^{15}N F_1 trace that would be derived from a "regular" TROSY experiment along with the resonance positions of each of the TROSY (Tr) and anti-TROSY (ATr) lines for the ground (A) and excited (B) states (black dots). The corresponding simulated D-evolution trace obtained using Δt = 1.0 ms and ν_{CPMG} = 300 Hz is shown in Figure 5b. If the TROSY component is not selected initially—as is the scenario in a typical TROSY scheme—the red spectrum is obtained, which clearly shows a shoulder close to the resonance position of the anti-TROSY component. This shoulder derives from magnetization that is initially of the anti-TROSY variety. It interferes with the accurate quantification of the position of the TROSY component of the major state and hence with the extraction of correct exchange parameters. In contrast, when the TROSY component is selected prior to the D-evolution element (blue curve) using an S^{3}E scheme as in the pulse sequence of Figure 4, for example, a symmetric peak is observed centered at the position expected for the exchange-modulated spin. As a further illustration of the influence of the anti-TROSY component (when it is not initially eliminated), consider the inset to the figure showing the case where the anti-TROSY component is selected initially and allowed to evolve under the D-evolution scheme, with selection of TROSY magnetization immediately prior to detection (green). It is clear that "contamination" from the initial anti-TROSY magnetization covers a range of frequencies that includes the resonance positions of the TROSY and anti-TROSY components and in between. The F_1 trace from the D-evolution TROSY sequence that omits the S^{3}E element is shown in red (inset; identical to the red trace in the main figure) for comparison.

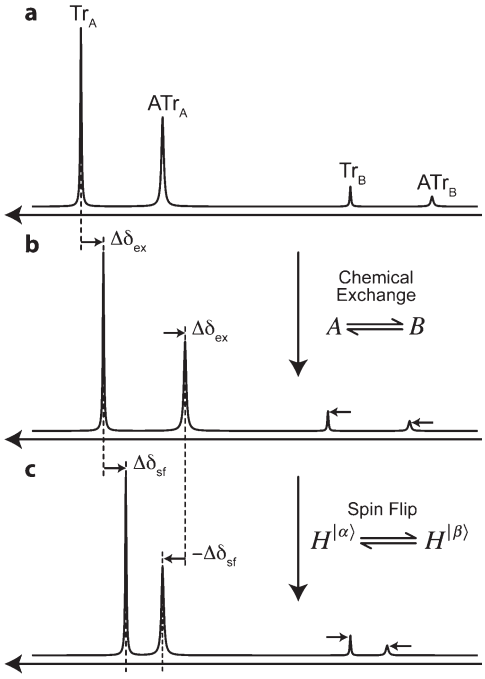

Figure 6. Schematic ^{15}N spectrum illustrating the shifts of the Tr and the ATr components of peaks A and B in an exchanging system, A ⇄ B (b), with interconversion between Tr and ATr components, $R_{sf} \neq 0$ (c). The case with no exchange (a) is shown as a reference. Chemical exchange moves the TROSY and anti-TROSY components of state "A" toward the corresponding lines in state "B", and vice versa by an amount $\Delta\delta_{ex}$, while for $R_{sf} \neq 0$ an additional shift of $\Delta\delta_{sf}$ for each line brings the TROSY and anti-TROSY components closer to each other. The shifts are additive in the case considered, but subtract when the relative positions of peaks from states A and B are reversed. In the D-evolution experiment both $\Delta\delta_{ex}$ and $\Delta\delta_{sf}$ depend on Δt and ν_{CPMG} in addition to the exchange parameters that they are sensitive to. In the illustrations it has been assumed that $k_{ex} \gg R_{sf}$, and no attempt has been made to show the exchange-induced contributions to the line widths.

The S^{3}E element described above effectively eliminates the asymmetric line shape issue that emerges from TROSY/anti-TROSY exchange. However, this exchange also leads to a second undesired effect—shifts of peak positions that cannot be

dx.doi.org/10.1021/ja109589y |J. Am. Chem. Soc. 2011, 133, 1935–1945

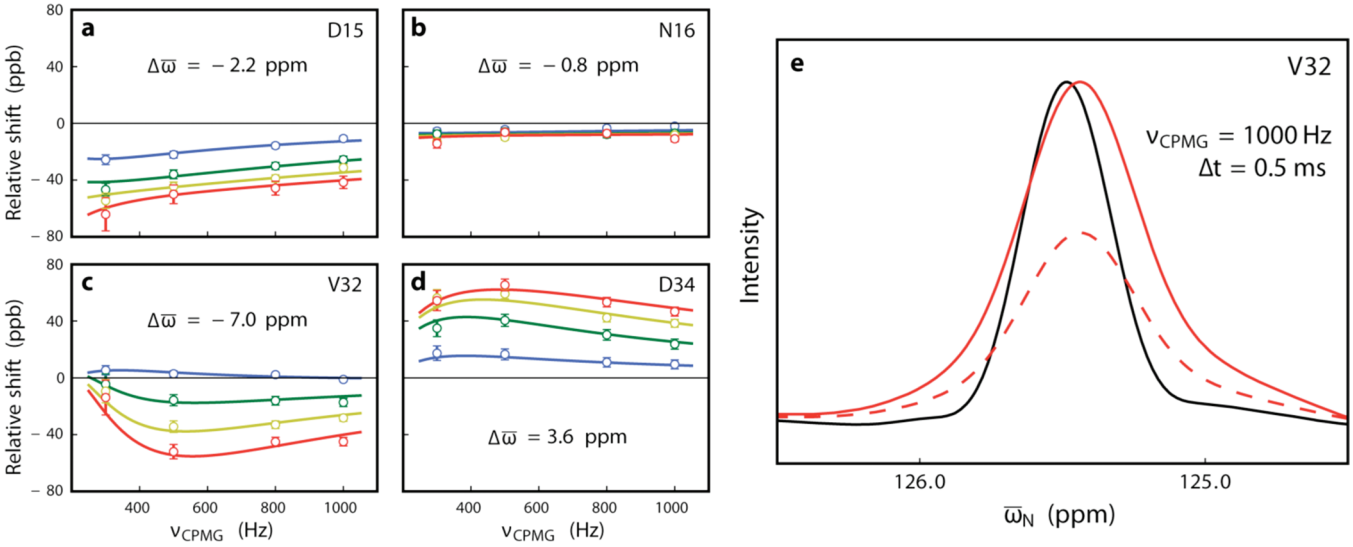

Figure 7. (a−d) Experimental ^{15}N relative shift profiles (circles) for Asp15, Asn16, Val32, and Asp34 of the Abp1p SH3/Ark1p peptide exchanging system, along with $\Delta\tilde{\omega}$ values extracted from the best fit to the data (solid lines). Data sets are recorded at a static field of 11.7 T for Δt = 2.2 (blue), 1.0 (green), 0.66 (yellow), and 0.5 (red) ms along with ν_{CPMG} varying from 300 to 1000 Hz. Errors are shown by vertical bars. (e) F_1 (^{15}N) traces for V32, extracted from 2D spectra recorded with Δt = 0.5 ms, with (red dashes, ν_{CPMG} = 1000 Hz) and without (black) the D-evolution element. The solid red spectrum has been scaled (from the red dashed spectrum) to have the same intensity as the trace recorded without D-evolution, making the shift in peak positions clear.

removed experimentally and that must, therefore, be accounted for in the analysis of the data. This is illustrated in Figure 6, where the four lines correspond to the TROSY and anti-TROSY components of the exchanging states A and B. When $k_{ex} \gg R_{sf}$, a situation that is very typically encountered, the effects of chemical exchange (k_{ex}) and exchange due to spin flips (**K** matrix above) can be separated to excellent approximation by first considering the much faster process that moves the position of the major state toward the minor state (eq 3), Figure 6b, followed by the slower process that repositions the major state TROSY line toward the anti-TROSY component and vice versa, Figure 6c. In the case where the ground-state spin resonates downfield of the excited-state spin (higher ppm for the ground state), both exchange processes are additive, as illustrated in Figures 6b,c, with a larger net shift obtained relative to the case where R_{sf} = 0. Conversely, a smaller shift is produced from these combined effects when the relative position of the ground- and excited-state peaks is reversed. It is noteworthy that the D-evolution scheme scales R_{sf}, much like k_{ex} and R_2 ($R_{sf}^{eff} = r_D R_{sf}$), so that the effective spin-flip rates can become substantial (R_{sf} is 1.5 s^{-1}, on average, for the exchanging system considered here at 25 °C with a maximum of 8.5 s^{-1} for D15; see below). Spin flips can be taken into account in the analysis of experimental data using eq 6, as has been done in the example that follows below.

Experimental Verification. To establish the utility of the D-evolution method for quantifying chemical exchange, we have considered an exchanging system described previously in which a small amount of a peptide (a 17-residue fragment from the yeast protein Ark1p) is added to the Abp1p SH3 domain.[24] When a small mole fraction of the peptide is included, the bound state is only marginally populated, corresponding to the excited state, with the ground state the peptide-free conformer. Experiments can be recorded on this protein−ligand exchanging system under these conditions and data analyzed to extract residue-specific values of $\Delta\omega$. These values can subsequently be compared with those obtained directly by recording spectra of ligand-free and fully bound SH3 domain to obtain some indication as to the robustness of the experiment. Parts a−d of Figure 7 illustrate a number of the D-evolution traces obtained for residues D15, N16, V32, and D34 of the Abp1p SH3/Ark1p peptide exchanging system (open circles), along with the best fits to the data using eq 6 (solid lines; see the Materials and Methods). Here a global model of two-site chemical exchange has been used, where all residues satisfying certain criteria (see the Materials and Methods) are included in the fit. In Figure 7e F_1 traces for V32 are shown, extracted from spectra recorded with Δt = 0.5 ms, with (red dashes, ν_{CPMG} = 1000 Hz) and without (black) the D-evolution element. Note the increased ^{15}N line width (decreased intensity, red dashes) that results from the D-evolution scheme. To emphasize the relative shift, the trace from the spectrum recorded with D-evolution is scaled to have the same intensity as the black trace; the resulting upfield shift is clear. It is worth reiterating that the sign of the chemical shift difference between exchanging states is obtained for "free", with negative $\Delta\omega$ values ($\omega_B - \omega_A$, i.e., excited − ground) for residues D15 (a; $\Delta\tilde{\omega}$ = −2.2 ppm), N16 (b; $\Delta\tilde{\omega}$ = −0.8 ppm), and V32 (c; $\Delta\tilde{\omega}$ = −7.0 ppm), while for D34 (d) $\Delta\tilde{\omega} > 0$ (3.6 ppm). Note that the relative shifts can be large in relation to the absolute shift in the free precession limit ($\Delta\delta_{ex}$, eq 3), where values of −8.1, −11.6, −2.8, and 5.3 ppb are calculated for the four residues in parts a−d, respectively, of Figure 7.

Even in cases where relative shifts are "large" they are less than 100 ppb (and often significantly less) so that care must be taken in ensuring that accurate peak positions can be obtained. Here we have used only well-resolved correlations that are fit using a program that considers the complete 2D line shape (see the Materials and Methods). Errors in peak positions are determined by the covariance matrix method[32] so that the accuracy of extracted frequencies can be established. For the set of 14 residues that were analyzed to extract $\Delta\tilde{\omega}$ values (using criteria discussed in the Materials and Methods), the average error in peak position is 3.3 ± 2.1 ppb for spectra recorded with Δt = 0.5 ms for which the

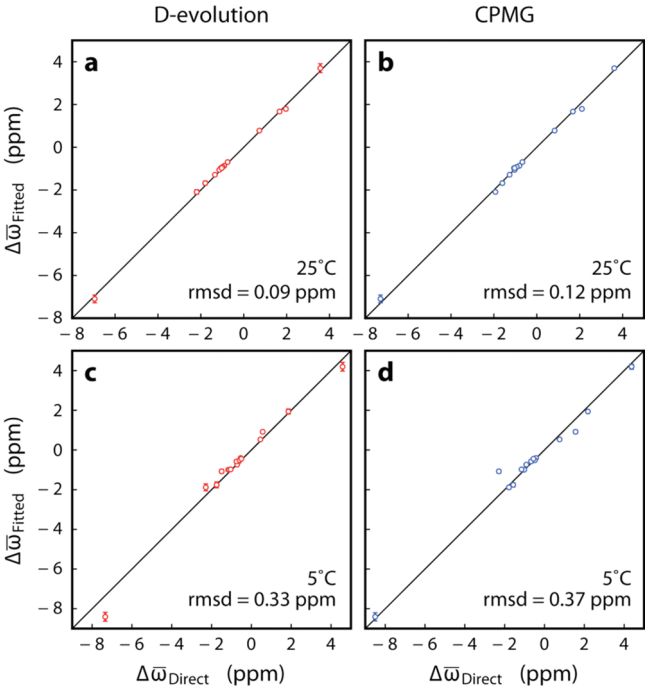

Figure 8. Correlation plots of ^{15}N chemical shift differences, $\Delta\tilde{\omega}_{\text{Fitted}}$, obtained from analysis of D-evolution (a, c) and CPMG (b, d) derived data sets recorded at 25 (a, b) and 5 (c, d) °C vs $\Delta\tilde{\omega}$ values (excited − ground) obtained directly from chemical shift measurements on samples of the free and fully bound SH3 domain, $\Delta\tilde{\omega}_{\text{Direct}}$. D-evolution $\Delta\tilde{\omega}$ values were extracted from relative shift profiles recorded at 11.7 T for Δt = 2.2, 1.0, 0.66, and 0.5 ms and with ν_{CPMG} varying from 300 to 1000 Hz. CPMG $\Delta\tilde{\omega}$ values were based on fits of dispersion curves recorded at 11.7 T (25 °C) and 11.7 and 18.8 T (5 °C). The same net measuring times were used in each class of experiments for each temperature. Points in red are those for which the sign of the $\Delta\tilde{\omega}_{\text{Fitted}}$ value is directly derived from the fit, while points in blue were signed a posteriori using the direct measurements.

scaling of the line width is largest and hence the signal-to-noise ratio is lowest (average S/N = 260 ± 130, 25 °C). An alternate estimate for the accuracy of peak positions can be obtained by noting that for residues where $\Delta\tilde{\omega} \approx 0$ ppm the extracted relative shift values are expected to be independent of ν_{CPMG}; rmsd values of experimental peak positions as a function of ν_{CPMG} for five residues that could be quantified accurately and that are not sensitive to ligand binding in the Abp1p SH3/Ark1p peptide exchanging system are small, between 1 and 2.5 ppb. The fact that errors are much less than the digital resolution (30 ms acquisition time in t_1) is consistent with previous studies of the accuracy of peak picking in cases where line shape analysis is used and high signal-to-noise data sets are evaluated.[28]

Figure 8 illustrates correlation plots of $\Delta\tilde{\omega}$ values obtained via D-evolution (a, c) and CPMG (b, d) methods vs $\Delta\tilde{\omega}$ generated directly from spectra recorded of the free or fully bound SH3 domain ($\Delta\tilde{\omega}_{\text{Direct}}$). For the D-evolution data, values of $\Delta\tilde{\omega}$ were extracted from fits of relative shift profiles recorded at a static magnetic field of 11.7 T for Δt values of 0.5, 0.66, 1.0, and 2.2 ms, along with ν_{CPMG} varying from 300 to 1000 Hz as indicated in Figure 7. Shift differences from the CPMG method were based on fits of dispersion curves recorded at 11.7 and 18.8 T. The same net measuring times were used in both classes of experiments to make the comparison in Figure 8 as "fair" as possible. The

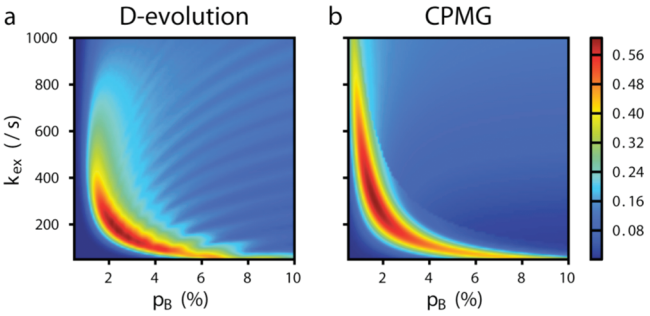

Figure 9. Surfaces of $P(p_B,k_{ex}) = \exp(-\chi^2/2\chi^2_{\text{min}})$ from fits of D-evolution (a) and CPMG (b) data sets recorded at 5 °C, where χ^2_{min} is the minimum of $\chi^2 = \sum_i[(X_i^{\text{exptl}} - X_i^{\text{calcd}}(p_B,k_{ex},\Delta\tilde{\omega}))^2/\sigma_i^2]$ and X_i is the relative shift (a) or $R_{2,\text{eff}}$ (b).

correlation is excellent for both the 25 and 5 °C data, although slightly worse at lower temperature. This may reflect the fact that exchange becomes relatively slow at 5 °C, making it more difficult to extract meaningful parameters. Values of (p_B, k_{ex}) = (2.6 ± 0.1%, 281 ± 10 s^{-1}) and (2.5 ± 0.1%, 298 ± 10 s^{-1}) were obtained from the D-evolution and CPMG approaches at 25 °C. The agreement between exchange parameters extracted from the D-evolution and CPMG data recorded at 5 °C, (p_B, k_{ex}) = (2.6 ± 0.1%, 151 ± 10 s^{-1}) and (1.9 ± 0.1%, 230 ± 13 s^{-1}), respectively, is less good. Note that the fraction of the ligand bound would not be expected to vary significantly with temperature given the high affinity of peptide for the SH3 domain[24] (0.55 ± 0.5 μM, 25 °C) and the low ligand concentration, while k_{ex} would be expected to decrease as the temperature is lowered. The (p_B, k_{ex}) values from the D-evolution data are thus physically reasonable, while those from the CPMG approach are suspect.

To explore this further, we have fitted the D-evolution (a) and CPMG (b) data sets recorded at 5 °C separately as a function of (p_B, k_{ex}). Shown in Figure 9 is the resultant probability surface, $P(p_B,k_{ex})$ (see the figure caption) where the optimal values of (p_B, k_{ex}) are those for which $P(p_B,k_{ex})$ is maximal. While there is clearly some interdependence between p_B and k_{ex} in both cases that complicates extraction of accurate values, as is expected when the exchange time scale is moderately slow ($k_{ex} \approx 150$ s^{-1}), the correlation is clearly stronger in fits of CPMG profiles. In the CPMG class of experiments only ν_{CPMG} is modified, with the exchange time scale effectively increasing as ν_{CPMG} becomes larger. In contrast, in the D-evolution scheme both Δt and ν_{CPMG} can be varied, making it "easier" to increase the exchange regime—and hence break/decrease the correlation between p_B and k_{ex}. This is one of the advantages of the D-evolution method over conventional relaxation dispersion experiments.

Probing Slower Exchange Time Scales. A strong motivation for the development of complementary methods to the CPMG relaxation dispersion experiment is to extend the window of exchange that is amenable for quantification to include slower time scales. To establish whether the D-evolution approach might be suitable in this regard, we have carried out a set of computations that compare this method with CPMG experiments for small values of k_{ex}. The D-evolution and CPMG schemes have been evaluated separately and then together for an "in silico" system exchanging with (p_B, k_{ex}) = (5%, 50 s^{-1}), Figure 10a−e, and with (p_B, k_{ex}) = (5%, 20 s^{-1}), Figure 10f−j. In both the D-evolution and CPMG simulations we have taken 15 residues from the Abp1p SH3/Ark1p peptide exchanging system that give rise to

dx.doi.org/10.1021/ja109589y |J. Am. Chem. Soc. 2011, 133, 1935–1945

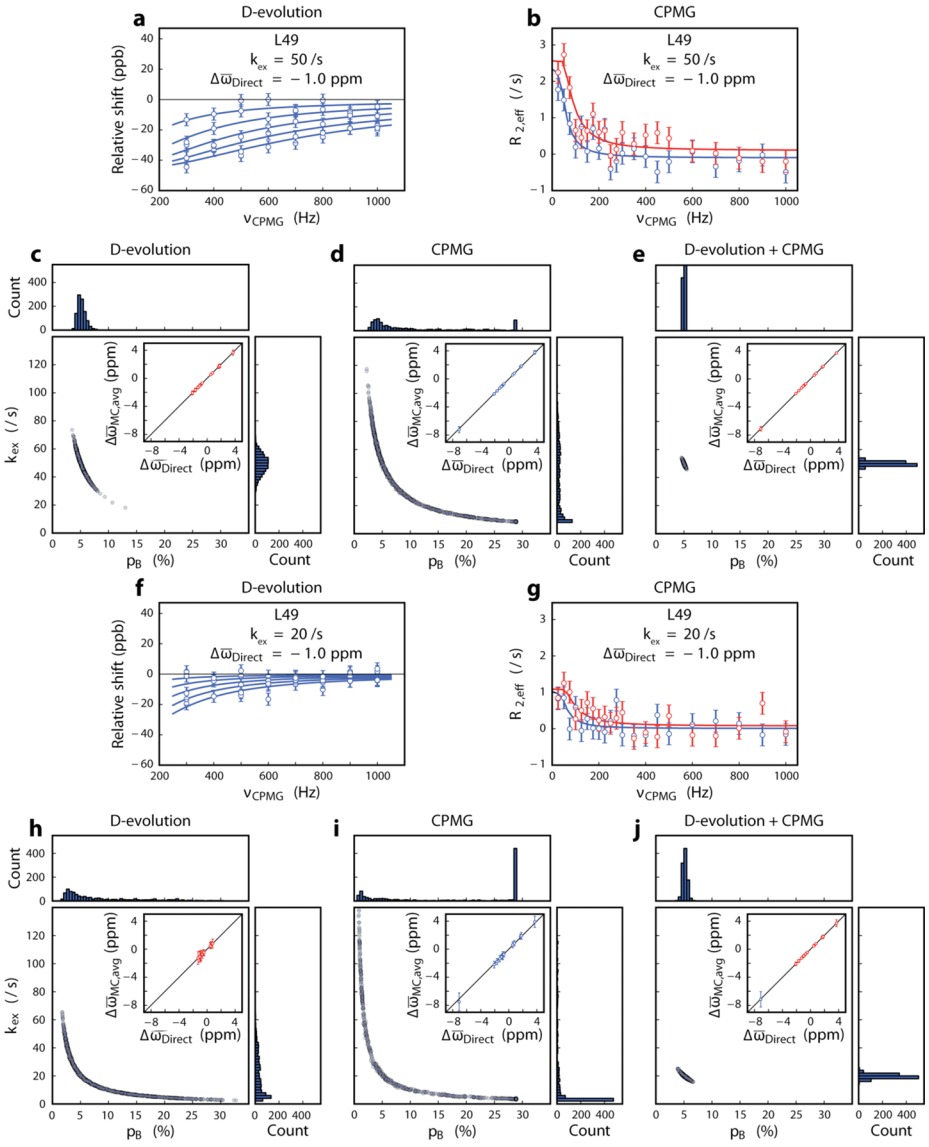

Figure 10. Complementarity between D-evolution and relaxation dispersion measurements for slow time scale exchange. A two-site exchanging system was simulated with $(p_B, k_{ex}) = (5\%, 50\ s^{-1})$, a—e, or $(p_B, k_{ex}) = (5\%, 20\ s^{-1})$, f—j. The system comprised 15 "residues", corresponding to those with the largest relative shifts (D-evolution simulations) or largest dispersion profiles (CPMG) from the Abp1p SH3 domain/Ark1p peptide complex that was studied experimentally, with $\Delta\tilde{\omega}$ (^{15}N) values taken directly from experiment. A total of 1000 synthetic D-evolution (11.7 T, Δt = 2.00, 1.14, 0.80, 0.62, and 0.50 ms) and CPMG (11.7 and 18.8 T) data sets were calculated via a Monte Carlo process whereby Gaussian noise with the same magnitude as the estimated experimental error (4 ppb, D-evolution; 0.3 s^{-1}, CPMG) is randomly added to the theoretical data. Examples of simulated D-evolution and CPMG profiles for one of the residues ($\Delta\tilde{\omega}$ = −1 ppm, corresponding to L49 of the Abp1p SH3 domain) are shown in (a), (b), (f), and (g). D-evolution and CPMG data sets were fitted independently (c, d and h, i) or together (e, j) to extract exchange parameters and chemical shift differences, with the distribution of (p_B, k_{ex}) values and histograms of k_{ex} (right panel) and p_B (top panel) as indicated. Correlation plots of $\Delta\tilde{\omega}_{MC,avg}$ (per residue $\Delta\tilde{\omega}$ values averaged over all simulations, with error bars denoting 1 standard deviation) and $\Delta\tilde{\omega}_{Direct}$ (the input $\Delta\tilde{\omega}$) are shown in the insets. In (a), (b), (f), and (g), blue and red denote data simulated for static magnetic fields of 11.7 and 18.8 T, while in all other panels red (blue) designate $\Delta\tilde{\omega}$ values where the sign was (was not) obtained correctly from fits of 99% of the data sets. Recall that sign information is not available from CPMG data (blue in (d) and (i)).

either the largest relative shifts (D-evolution) or the largest dispersion profiles (CPMG) and used the corresponding $\Delta\tilde{\omega}$ values (obtained via direct measurement) and errors that are obtained from experiment. Note that there is some but not complete overlap between the D-evolution and CPMG sets of residues at a given (p_B, k_{ex}) and the residues chosen do vary between the two sets of (p_B, k_{ex}) that have been selected in the computations. D-evolution and CPMG data sets are simulated for these 15 residues to closely reproduce the experiment; D-evolution profiles are computed for Δt values of 2.00, 1.14, 0.80, 0.62, and 0.50 ms (11.7 T), while CPMG curves are generated for fields of 11.7 and 18.8 T. The number of points and profiles "chosen" is such that both D-evolution and CPMG data would be recorded in similar measurement times. A total of 1000 data sets are generated via a Monte Carlo process whereby Gaussian noise, with the same magnitude as the estimated experimental error (see the discussion above), is randomly added to the theoretical data,[32] and each of the 1000 data sets are fitted

dx.doi.org/10.1021/ja109589y |J. Am. Chem. Soc. 2011, 133, 1935–1945

globally to extract (p_B, k_{ex}) along with $\Delta\tilde{\omega}$ values for each residue. Parts a and b (f and g) of Figure 10 show representative simulated "relative shift" and CPMG profiles for $\Delta\tilde{\omega}=-1.0$ ppm (corresponding to Leu 49 of the Abp1p SH3 domain). Parts c and d (h and i) plot (p_B, k_{ex}) distributions obtained from global fits of the sets of D-evolution (c, h) or CPMG (d, i) profiles, along with correlation plots of $\Delta\tilde{\omega}_{MC,avg}$ (extracted from fits of simulated data and reported as an average over all simulations, with error bars denoting 1 standard deviation) and $\Delta\tilde{\omega}_{Direct}$ (the input $\Delta\tilde{\omega}$). It is clear that (p_B, k_{ex}) distributions are more accurate when obtained from the D-evolution data. For example, from the simulated data sets with (p_B, k_{ex}) = (5%, 50 s^{-1}), values of $(p_B, k_{ex})_{avg}$ = (5.2 ± 0.8%, 49 ± 7 s^{-1}) and (11.0 ± 8.6%, 39 ± 25 s^{-1}) are extracted from fits of the D-evolution and CPMG data, respectively. In a similar manner, for simulations with (p_B, k_{ex}) = (5%, 20 s^{-1}) the values for $(p_B, k_{ex})_{avg}$ are (9.1 ± 7.3%, 20 ± 15 s^{-1}) and (17.3 ± 12.0%, 24 ± 35 s^{-1}). Further analysis of the fits establishes that, while exchange parameters are more robustly extracted from D-evolution data sets, values of $\Delta\tilde{\omega}$ are more accurate when obtained from fits of CPMG profiles. To quantify the accuracy of extracted chemical shift differences, each of the 1000 correlation plots, $\Delta\tilde{\omega}_{MC}$ vs $\Delta\tilde{\omega}_{Direct}$, has been fitted to extract a slope; averages of 0.98 ± 0.12 and 1.02 ± 0.05 are obtained from the D-evolution and CPMG data generated with (p_B, k_{ex}) = (5%, 50 s^{-1}), while 1.03 ± 0.75 and 1.06 ± 0.13 are calculated when (p_B, k_{ex}) = (5%, 20 s^{-1}). Although the average values of the slopes are all close to 1, the substantial standard deviation for D-evolution data when k_{ex} = 20 s^{-1}, in particular, clearly indicates that at least some of the $\Delta\tilde{\omega}$ values will be determined incorrectly for small exchange rates. The very significant complementarity between the two classes of experiments is made clear in parts e and j of Figure 10, where the combined CPMG and D-evolution data sets are fitted to extract very accurate (p_B, k_{ex}) {$(p_B, k_{ex})_{avg}$ = (5.0 ± 0.1%, 50 ± 1 s^{-1}) and (5.2 ± 0.4%, 20 ± 1 s^{-1})} and $\Delta\tilde{\omega}$ (average slope of $\Delta\tilde{\omega}_{MC}$ vs $\Delta\tilde{\omega}_{Direct}$ profiles 1.00 ± 0.03 and 1.01 ± 0.09 for (p_B, k_{ex}) = (5%, 50 s^{-1}) and (p_B, k_{ex}) = (5%, 20 s^{-1}), respectively) values. That such accurate parameters can be obtained in the combined analysis indicates that the (p_B, k_{ex}, $\Delta\tilde{\omega}_i$) surfaces generated separately from fits of CPMG and D-evolution profiles are not collinear, despite the fact that the (p_B, k_{ex}) curves in Figure 10 are similar. Further, the simulations presented indicate that the pronounced correlation between p_B and k_{ex} that manifests in the slow exchange regime can be very significantly broken by a combination of CPMG and D-evolution experiments. This, no doubt, reflects the fact that the contributions to $R_{2,eff}$ and the relative shift from slow exchange processes are given, to first order, by $p_B k_{ex}$ and $p_A p_B k_{ex}(k_{ex}/\Delta\omega)$, respectively, which depend in different ways on p_B and k_{ex}.

Concluding Remarks. We have presented a new experiment for quantifying millisecond time scale chemical exchange in protein systems. The experiment is based on manipulation of peak positions as opposed to transverse relaxation rates. Its utility is highest where the exchange time scale can be "swept" from slow/intermediate to fast. For large values of k_{ex}, such that $k_{ex} \gg \Delta\omega$, the exchange time scale is fast even without scaling and little effect is observed. In contrast, for k_{ex} on the order of or smaller than $\Delta\omega$, larger effects are noted. A range of exchange scenarios is likely to be encountered in many exchanging proteins since many different exchanging spins, with different $\Delta\tilde{\omega}$ values, will be involved. The goal of the present work has not been to develop a scheme that replaces the CPMG experiment, but rather that complements it. For example, (i) in the D-evolution experiment the sign of $\Delta\omega$ is obtained directly, unlike in CPMG data sets that are only sensitive to $|\Delta\omega|$, and (ii) simulations establish that more robust measures of p_B and k_{ex} can be extracted from D-evolution data in cases where exchange is in the slow regime. This is borne out experimentally by the Abp1p SH3/Ark1p peptide data at 5 °C, where (p_B, k_{ex}) values are most certainly in error when obtained from fits of CPMG profiles, while exchange parameters from the D-evolution experiments are more reasonable. Interestingly, accurate $\Delta\tilde{\omega}$ values are obtained at 5 °C via both methods, although simulations clearly establish that as exchange rates become increasingly small $\Delta\tilde{\omega}$ values from fits of CPMG data are more accurate than from D-evolution profiles. A disadvantage at present is that, unlike the CPMG experiment, which has been successfully applied in studies of very high molecular weight proteins and protein complexes,[30,33−35] the D-evolution scheme is limited to applications involving small proteins since intrinsic line widths are scaled by the same factor as exchange rates, decreasing spectral resolution. Put another way, the long net effective evolution period, $t_1 + T_{CPMG}$, for each point places limitations on the sizes of molecules that are currently amenable for study, with an upper limit of approximately 10−15 kDa. It may be that more sophisticated pulse schemes that place magnetization along the z-axis for a fraction of the evolution period will prove to be advantageous.[36] Where possible, it seems likely that analysis of some combination of both CPMG and D-evolution data sets will be the most robust approach for obtaining accurate exchange parameters and chemical shift values. A major result of the present study, albeit only established via computation at this point, is that a joint analysis of CPMG and D-evolution profiles leads to an increase in the window of exchange processes that can be studied in detail. Accurate (p_B, k_{ex}) and $\Delta\tilde{\omega}$ values were simulated for k_{ex} values as low as 20 s^{-1} (p_B = 5%), which is an approximate order of magnitude lower in exchange time scale than is typically studied by CPMG relaxation dispersion. The scheme presented here adds to a growing list of experiments for quantifying chemical exchange in proteins to facilitate increasingly accurate descriptions of excited protein states.

MATERIALS AND METHODS

Sample Preparation. [U-^{15}N,^{2}H]Abp1p SH3 domain was expressed and purified as previously described.[24] The final protein concentration used for NMR analyses was ~1.5 mM, in a buffer consisting of 50 mM sodium phosphate, 100 mM NaCl, 1 mM EDTA, 1 mM NaN_3, 90% H_2O/10% D_2O, pH 7.0. Ark1p peptide[37] was prepared as detailed in a previous publication[24] and added to the Abp1p SH3 domain sample to produce a complex with 2.5 ± 0.1% mole fraction bound peptide, as established by ^{15}N CPMG relaxation dispersion experiments.[11]

NMR Spectroscopy

1. Pulse Sequence Details (Figure 4). ^{1}H and ^{15}N 90° (180°) pulses are shown as narrow (wide) black bars and are applied at the highest possible power levels, with the exception of the ^{15}N refocusing pulses of the CPMG elements (gray boxes) as well as the ^{15}N 90° pulse preceding the t_1 evolution period that are applied at a lower power level (~4.5 kHz). The ^{1}H inversion pulse in gray is applied as $90°_y-180°_x-90°_y$ (ref38). The shaped 90° ^{1}H pulses are water-selective (~1.5 ms). All pulse phases are assumed to be x, unless indicated otherwise. The refocusing pulses of the CPMG blocks of the D-evolution element follow a standard XY-4 {x, y, x, y} phase cycle that is supercycled along with each dwell time according to an XY-16 scheme,[27] ϕ_4 = {$X, Y, X, Y, Y, X, Y, X, -X, -Y, -X, -Y, -Y, -X, -Y, -X$}, where X = XY-4 and

dx.doi.org/10.1021/ja109589y |J. Am. Chem. Soc. 2011, 133, 1935–1945

$Y = YX$-4. Thus, immediately after the first Δt, the cycle for the four refocusing pulses is x, y, x, y, corresponding to the first X in ϕ_4. After the second Δt, the cycle is y, x, y, x, corresponding to the first Y in ϕ_4, and so forth. We have also tried a simpler scheme, $\Delta t-(x,y,x,y)-\Delta t-(y,x,y,x)-\Delta t-(-x,-y,-x,-y)-\Delta t-(-y,-x,-y,-x)-\Delta t-(x,y,x,y)-...$, that appears equally good. The rest of the phase cycling used is as follows (Varian): $\phi_1 = 4\{-x\}, 4\{x\}$; $\phi_2 = \{45°\}$; $\phi_3 = 2\{y\}, 2\{-y\}, 2\{x\}, 2\{-x\}$; $\phi_5 = \{-y\}$; $\phi_6 = \{y\}$; $\phi_7 = \{-y\}$; $\phi_8 = \{x, -x\}$; $\phi_9 = \{-x, x\}$; receiver = $2\{y\}, 2\{-y\}, 2\{x\}, 2\{-x\}$. Quadrature detection in the indirect dimension is obtained by the enhanced sensitivity approach[39,40] by recording a second spectrum where ϕ_5, ϕ_6, and ϕ_7 are inverted along with the phase of the receiver and $\phi_3 = 2\{y\}, 2\{-y\}, 2\{-x\}, 2\{x\}$ for each t_1 increment. In addition, both phase ϕ_3 and the phase of the receiver are incremented by 180° for every complex t_1 point (in the States-TPPI manner[41]). The delays used are $\tau_a = 2.3$ ms and $\tau_b = 1/(8J_{NH}) = 1.36$ ms. Gradient strengths, G/cm (length, ms) are $g_0 = 6.0$ (1.0), $g_1 = 5.5$ (1.0), $g_2 = 6.0$ (1.0), $g_3 = 14.0$ (0.3), $g_4 = 26.0$ (0.5), $g_5 = 8.0$ (0.8), $g_6 = 15.0$ (1.0), $g_7 = 6.4$ (0.4), and $g_8 = 40.0$ (0.2). A CPMG block of varying length ($N_1/4 = N_{max} - N + 1$) is applied at the beginning of the sequence so that the extent of heating is constant over all measurements. In the absence of such an element, sample heating increases slightly as a function of t_1, giving rise to peaks whose line shapes are distorted, significantly affecting the accuracy by which peak positions can be quantified. This distortion is completely removed when the initial CPMG block is used. When the reference spectrum (standard evolution instead of D-evolution) is recorded, $N_1/4$ is set to $N_{max} + 1$ for all t_1 increments and the $(-\tau-180_\phi-\tau-)_4$ block is removed.

2. Experimental Details. ^{15}N relative shift profiles of the Abp1p SH3/Ark1p exchanging complex were obtained at a static magnetic field strength of 11.7 T at both 25 and 5 °C using the D-evolution TROSY experiment illustrated in Figure 4. The relative shift, $\delta_a - \delta_b$, is defined as the peak position in spectra recorded with (δ_a) and without (δ_b) the $(-\tau-180_\phi-\tau-)_4$ element of Figure 4 (element contained in the second shaded box). Spectra were measured with dwell times, Δt, of 2.2 ($N_{max} = 52$, where N_{max} is the number of complex t_1 points; see Figure 4), 1.0 ($N_{max} = 60$), 0.66 ($N_{max} = 60$), and 0.5 ($N_{max} = 60$) ms. Each data set was recorded with four (at 25 °C) or seven (at 5 °C) ν_{CPMG} [$=1/(4\tau)$] values, ranging from 300 to 1000 Hz. A pair of reference spectra (without D-evolution) were obtained for each dwell time. Each plane was recorded with an acquisition time of 128 ms in the direct dimension along with a prescan delay of 3.0 s, so that total acquisition times for all of the data were 22 and 32.5 h at 25 and 5 °C, respectively. To account for any heating effects, a CPMG block of varying length was applied at the beginning of the sequence so that the power used for each increment remains the same. In addition, planes sharing the same dwell time were recorded in a pseudo-3D manner whereby data sets with different ν_{CPMG} values were interleaved to further equilibrate heating over the different planes.

^{15}N CPMG relaxation dispersion profiles[11] were obtained for the Abp1p SH3/Ark1p complex at static magnetic field strengths of 11.7 T at 25 °C and 11.7 and 18.8 T at 5 °C. Totals of 24 (11.7 T, 25 °C), 22 (11.7 T, 5 °C), and 21 (18.8 T, 5 °C) ν_{CPMG} values ranging from 25 to 1000 Hz ($T_{relax} = 40$ ms) were measured. Data sets were recorded with acquisition times of (47, 64) ms at (11.7 T, 25 °C), (40, 64) ms at (11.7 T, 5 °C), and (33, 64) ms at (18.8 T, 5 °C) in (t_1, t_2), along with a prescan delay of 2.5 s, for total acquisition times of 18.5, 16.5, and 18.5 h, respectively.

Data Analysis. All data sets were processed and analyzed with the NMRPipe program.[42] As described in the text, relative shift profiles, $\Delta\delta^{exptl}(\Delta t, \nu_{CPMG})$, were generated by calculating the differences in chemical shifts between peaks in reference spectra and their counterparts in each D-evolution correlation map measured as a function of Δt and ν_{CPMG}. Peak positions were quantified using the program FuDA (http://pound.med.utoronto.ca/software.html), using a model in which peaks were assumed to be a mixture of Gaussian and Lorentzian line shapes. All the planes with the same dwell time, Δt, were fitted together, assuming identical (different) peak positions and line shapes in the direct (indirect) dimension and the same peak volume over the planes. Errors in peak positions were estimated on the basis of either the covariance matrix[32] of the fit or duplicate measurements when available. Errors in relative shift values were calculated as the Euclidian norm of the reference and D-evolution shift errors.

Relative shift profiles were analyzed using a two-site exchange model, and values of k_{ex}, p_B, and $\Delta\tilde{\omega}$ were extracted from the simultaneous (global) fit of the data from all residues with an average relative shift (averaged over all Δt and ν_{CPMG} values) greater than both 2 times the average error and 5 ppb. Shifts from strongly overlapped peaks were excluded from the analysis. Data were fitted using in-house-written software by minimization of the following χ^2 target function:

$$\chi^2(\zeta) = \sum \left(\frac{\Delta\delta^{calcd}(\zeta) - \Delta\delta^{exptl}}{\Delta\Delta\delta^{exptl}} \right)^2 \quad (7)$$

where $\Delta\delta^{exptl}$ and $\Delta\Delta\delta^{exptl}$ are experimental relative shifts and their uncertainties, respectively, $\Delta\delta^{calcd}(\zeta)$ are relative shifts calculated as described below, $\zeta = \{x_1, ..., x_{npar}\}$ denotes the set of adjustable model parameters, and the summation is over all the experimental data points.

Values of $\Delta\delta^{calcd} = \delta_a - \delta_b$ were computed by calculating peak positions of the major state (A) with (δ_a) and without (δ_b) the D-evolution element. Values of δ_b are obtained by calculating eigenvalues of the 4×4 matrix

$$\mathbf{\Lambda}_{4\times4} = \begin{bmatrix} \mathbf{\Lambda}_{TR} & \mathbf{K} \\ \mathbf{K} & \mathbf{\Lambda}_{ATr} \end{bmatrix} \quad (8)$$

and noting that the chemical shift of interest is given by the imaginary part of the eigenvalue corresponding to the TROSY component of state A. In turn, δ_a can be calculated by first noting that, when the D-evolution element is included, the propagator describing the evolution of magnetization over a single dwell period is given by an expression similar to eq 4:

$$P = \{\exp(\mathbf{\Lambda}_{4\times4}\tau)\exp(\mathbf{\Lambda}^*_{4\times4}2\tau)\exp(\mathbf{\Lambda}_{4\times4}\tau)\}^2 \exp(\mathbf{\Lambda}_{4\times4}\Delta t) \quad (9)$$

where $\mathbf{\Lambda}^*_{4\times4}$ is the complex conjugate of $\mathbf{\Lambda}_{4\times4}$. The average Liouvillian, $\boldsymbol{L}^{avg}_{4\times4}$, describing the time dependence of magnetization in the presence of the D-evolution element is then given by[43]

$$\boldsymbol{L}^{avg}_{4\times4} = \ln(P)/\Delta t \quad (10)$$

with δ_a obtained from the appropriate eigenvalue of $\boldsymbol{L}^{avg}_{4\times4}$, as described above.

Values of R_{sf}, reflecting the TROSY/anti-TROSY interconversion, have been measured experimentally by recording the decay of both ^{15}N longitudinal magnetization (R_1) and ^{15}N$-^1$H^N longitudinal order (R_{zz}), $R_{sf} = R_{zz} - R_1$. These rates were then used directly in the expression for $\mathbf{\Lambda}_{4\times4}$ in fits of D-evolution data. We have not included differences in TROSY and anti-TROSY relaxation rates in any of the analyses; such differences enter only indirectly through spin flips and will make small contributions for the relatively small proteins for which the D-evolution methodology is applicable. Simulations have established that, for the Abp1p SH3 domain/Ark1p peptide exchanging system considered here, where average rates for R_{sf}, $R_{2,TR}$, and $R_{2,ATr}$ are 1.5, 1.5, and 8.9 s^{-1}, respectively, differences between $R_{2,TR}$ and $R_{2,ATr}$ do not affect relative shift values by more than 0.02 ppb on average, with a maximum of 0.6 ppb for D15, where the largest R_{sf} rate is measured (8.5 s^{-1}). If desired, values of $R_{2,TR}$ can be obtained from plateaus of ^{15}N TROSY CPMG dispersion profiles[30] and measured R_{sf} rates; $R_{2,ATr}$ can then be calculated directly from $R_{2,TR}$ assuming standard parameters for ^{15}N CSA values and ^{1}H$-^{15}$N bond lengths. Finally, in the study reported here errors in the extracted exchange parameters were estimated by the covariance matrix method.[32]

CPMG relaxation dispersion profiles, $R_{2,\mathrm{eff}}(\nu_{\mathrm{CPMG}})$, were generated from peak intensities, $I_1(\nu_{\mathrm{CPMG}})$, in a series of 2D $^1H^N-^{15}N$ correlation maps measured as a function of CPMG frequency, ν_{CPMG}. Effective relaxation rates were calculated as $R_{2,\mathrm{eff}}(\nu_{\mathrm{CPMG}}) = \ln(I_0/I_1(\nu_{\mathrm{CPMG}}))/T_{\mathrm{relax}}$, where I_0 is the peak intensity in the reference spectrum recorded without the relaxation delay T_{relax} (refs 12 and 44). Signal intensities were quantified using the program FuDA. Relaxation dispersion data were analyzed using a two-state exchange model, and the best fit model parameters were extracted as described previously[14] using the program CATIA, which is available from http://pound.med.utoronto.ca/software.html.

■ ASSOCIATED CONTENT

Supporting Information. Complete author list for ref 7. This material is available free of charge via the Internet at http://pubs.acs.org.

■ AUTHOR INFORMATION

Corresponding Author

kay@pound.med.utoronto.ca; d.hansen@ucl.ac.uk

Present Addresses

[†]Institute of Structural and Molecular Biology, University College London, London WC1E 6BT, United Kingdom.

■ ACKNOWLEDGMENT

G.B. acknowledges the European Molecular Biology Organization and the Canadian Institutes of Health Research (CHIR) for postdoctoral fellowships. D.F.H. was supported by a postdoctoral fellowship from the CIHR. This work was supported by a grant from the CIHR. L.E.K. holds a Canada Research Chair in Biochemistry.

■ REFERENCES

(1) Carr, H. Y.; Purcell, E. M. *Phys. Rev.* **1954,** *54*, 630–638.
(2) Meiboom, S.; Gill, D. *Rev. Sci. Instrum.* **1958,** *29*, 688–691.
(3) Palmer, A. G.; Kroenke, C. D.; Loria, J. P. *Methods Enzymol.* **2001,** *339*, 204–238.
(4) Korzhnev, D. M.; Kay, L. E. *Acc. Chem. Res.* **2008,** *41*, 442–51.
(5) Boehr, D. D.; McElheny, D.; Dyson, H. J.; Wright, P. E. *Science* **2006,** *313*, 1638–42.
(6) Eisenmesser, E. Z.; Millet, O.; Labeikovsky, W.; Korzhnev, D. M.; Wolf-Watz, M.; Bosco, D. A.; Skalicky, J. J.; Kay, L. E.; Kern, D. *Nature* **2005,** *438*, 117–21.
(7) Shen, Y.; et al. *Proc. Natl. Acad. Sci. U.S.A.* **2008,** *105*, 4685–90.
(8) Cavalli, A.; Salvatella, X.; Dobson, C. M.; Vendruscolo, M. *Proc. Natl. Acad. Sci. U.S.A.* **2007,** *104*, 9615–20.
(9) Wishart, D. S.; Arndt, D.; Berjanskii, M.; Tang, P.; Zhou, J.; Lin, G. *Nucleic Acids Res.* **2008,** *36*, W496–502.
(10) Loria, J. P.; Rance, M.; Palmer, A. G. *J. Am. Chem. Soc.* **1999,** *121*, 2331–2332.
(11) Hansen, D. F.; Vallurupalli, P.; Kay, L. E. *J. Phys. Chem.* **2008,** *112*, 5898–5904.
(12) Tollinger, M.; Skrynnikov, N. R.; Mulder, F. A. A.; Forman-Kay, J. D.; Kay, L. E. *J. Am. Chem. Soc.* **2001,** *123*, 11341–11352.
(13) Ishima, R.; Torchia, D. *J. Biomol. NMR* **2003,** *25*, 243–248.
(14) Hansen, D. F.; Vallurupalli, P.; Lundstrom, P.; Neudecker, P.; Kay, L. E. *J. Am. Chem. Soc.* **2008,** 2667–2675.
(15) Ishima, R.; Baber, J.; Louis, J. M.; Torchia, D. A. *J. Biomol. NMR* **2004,** *29*, 187–98.
(16) Lundstrom, P.; Hansen, D. F.; Kay, L. E. *J Biomol NMR* **2008,** *42*, 35–47.
(17) Lundstrom, P.; Kay, L. E. *J. Biomol. NMR* **2009,** *44*, 139–55.
(18) Lundstrom, P.; Hansen, D. F.; Vallurupalli, P.; Kay, L. E. *J. Am. Chem. Soc.* **2009,** *131*, 1915–26.
(19) Korzhnev, D. M.; Religa, T. L.; Banachewicz, W.; Fersht, A. R.; Kay, L. E. *Science* **2010,** *329*, 1312–6.
(20) Skrynnikov, N. R.; Dahlquist, F. W.; Kay, L. E. *J. Am. Chem. Soc.* **2002,** *124*, 12352–60.
(21) Anet, F. A.; Basus, V. J. *J. Magn. Reson.* **1978,** *32*, 339–343.
(22) Morris, G. A.; Jerome, N. P.; Lian, L. Y. *Angew. Chem., Int. Ed.* **2003,** *42*, 823–5.
(23) Zhuravleva, A.; Orekhov, V. Y. *J. Am. Chem. Soc.* **2008,** *130*, 3260–1.
(24) Vallurupalli, P.; Hansen, D. F.; Stollar, E. J.; Meirovitch, E.; Kay, L. E. *Proc. Natl. Acad. Sci. U.S.A.* **2007,** *104*, 18473–18477.
(25) Pervushin, K.; Riek, R.; Wider, G.; Wüthrich, K. *Proc. Natl. Acad. Sci. U.S.A.* **1997,** *94*, 12366–12371.
(26) Meissner, A.; Duus, J. O.; Sorensen, O. W. *J Biomol. NMR* **1997,** *10*, 89–94.
(27) Gullion, T.; Baker, D. B.; Conradi, M. S. *J. Magn. Reson.* **1990,** *89*, 479–484.
(28) Kontaxis, G.; Clore, G. M.; Bax, A. *J. Magn. Reson.* **2000,** *143*, 184–96.
(29) Goldman, M. *J. Magn. Reson.* **1984,** *60*, 437–452.
(30) Loria, J. P.; Rance, M.; Palmer, A. G. *J. Biomol. NMR* **1999,** *15*, 151–155.
(31) Hansen, D. F.; Vallurupalli, P.; Kay, L. E. *J. Am. Chem. Soc.* **2008,** *130*, 8397–405.
(32) Press, W. H.; Flannery, B. P.; Teukolsky, S. A.; Vetterling, W. T. *Numerical Recipes in C*; Cambridge University Press: Cambridge, U.K., 1988.
(33) Palmer, A. G.; Grey, M. J.; Wang, C. *Methods Enzymol.* **2005,** *394*, 430–65.
(34) Korzhnev, D. M.; Kloiber, K.; Kay, L. E. *J. Am. Chem. Soc.* **2004,** *126*, 7320–9.
(35) Sprangers, R.; Kay, L. E. *Nature* **2007,** *445*, 618–22.
(36) Li, Y.; Palmer, A. G., III. *J. Am. Chem. Soc.* **2010,** *132*, 8856–7.
(37) Haynes, J.; Garcia, B.; Stollar, E. J.; Rath, A.; Andrews, B. J.; Davidson, A. R. *Genetics* **2007,** *176*, 193–208.
(38) Levitt, M.; Freeman, R. *J. Magn. Reson.* **1978,** *33*, 473–476.
(39) Kay, L. E.; Keifer, P.; Saarinen, T. *J. Am. Chem. Soc.* **1992,** *114*, 10663–10665.
(40) Schleucher, J.; Sattler, M.; Griesinger, C. *Angew. Chem., Int. Ed. Engl.* **1993,** *32*, 1489–1491.
(41) Marion, D.; Ikura, M.; Tschudin, R.; Bax, A. *J. Magn. Reson.* **1989,** *85*, 393–399.
(42) Delaglio, F.; Grzesiek, S.; Vuister, G. W.; Zhu, G.; Pfeifer, J.; Bax, A. *J. Biomol. NMR* **1995,** *6*, 277–293.
(43) Ernst, R. R.; Bodenhausen, G.; Wokaun, A. *Principles of Nuclear Magnetic Resonance in One and Two Dimensions*; Oxford University Press: Oxford, U.K., 1987.
(44) Mulder, F. A. A.; Skrynnikov, N. R.; Hon, B.; Dahlquist, F. W.; Kay, L. E. *J. Am. Chem. Soc.* **2001,** *123*, 967–975.